

Stochastic Geometry Analysis of Multi-Antenna Two-Tier Cellular Networks

Zheng Chen, Ling Qiu, *Member, IEEE*, and Xiaowen Liang

Abstract—In this paper, we study the key properties of multi-antenna two-tier networks under different system configurations. Based on stochastic geometry, we derive the expressions and approximations for the users' average data rate. Through the more tractable approximations, the theoretical analysis can be greatly simplified. We find that the differences in density and transmit power between two tiers, together with range expansion bias significantly affect the users' data rate. Besides, for the purpose of area spectral efficiency (ASE) maximization, we find that the optimal number of active users for each tier is approximately fixed portion of the sum of the number of antennas plus one. Interestingly, the optimal settings are insensitive to different configurations between two tiers. Last but not the least, if the number of antennas of macro base stations (MBSs) is sufficiently larger than that of small cell base stations (SBSs), we find that range expansion will improve ASE.

Index Terms—Area spectral efficiency, heterogeneous networks, multi-antenna base stations, stochastic geometry.

I. INTRODUCTION

HETEROGENEOUS networks (HetNets), which is composed of MBSs overlaid with SBSs, has been recognized as a promising approach to cope with the 1000x traffic demand [1]. However, the differences in transmit power and BS density between MBSs and SBSs make the properties of HetNets different from the traditional single-tier networks.

To characterize the performance of HetNets, stochastic geometry has been identified as a powerful tool because of its accuracy and tractability. By modeling MBSs and SBSs as independent Poisson point processes (PPPs), the performance of HetNets has been extensively studied in [2][3][4]. Especially, the technique of cell range expansion for load-balancing was considered in [4]. It is found that, although range expansion improves the fairness between users, the overall throughput will be degraded. However, [2][3][4] only considered single-antenna BSs, the key properties of multi-antenna HetNets cannot be revealed. In multi-antenna single-tier networks, the ASE and energy efficiency have been studied in [5][6]. [7] analyzed the error probability of single-tier Poisson distributed networks. However, the interplay between different tiers in HetNets cannot be understood in [5][6][7]. To take a step further, the coverage probability of multi-antenna HetNets was investigated in [8][10][9]. [11] studied the coverage probability of multi-antenna HetNets with transmit-receive diversity. However, [8][10][9][11] focused more on

the analysis of signal-to-interference-plus-noise-ratio (SINR), which is usually in complex form. It is difficult to analyze the properties of multi-antenna HetNets under different system parameters theoretically based on the previous works. As a results, the impact of differences between two tiers on system performance have not been well investigated.

In this paper, we derive the expressions and tight approximations for users' average data rate in multi-antenna two-tier networks. Through the more tractable approximations, we study how different system parameter configurations affect the users' average data rate theoretically. Furthermore, also based on the approximations, we obtain the optimal number of active users of each tier to maximize ASE. We study the optimal settings under different system parameters. We find that the ratio of BS density and transmit power $\frac{\lambda_s}{\lambda_m}, \frac{P_s}{P_m}$ and the range expansion bias mainly affect the users' data rate and the optimal settings.¹ Moreover, the results based on the approximations are validated through numerical results. The novel and insightful findings of this paper as follows:

- The average data rate of macro or small cell users is insensitive to the number of active users of the other tier. If range expansion is considered, the users' data rates of both tier increase with $\frac{\lambda_s}{\lambda_m}, \frac{P_s}{P_m}$. However, if range expansion is not considered, the users' data rate is insensitive to $\frac{\lambda_s}{\lambda_m}, \frac{P_s}{P_m}$.
- For each tier, the ratio between the optimal number of active users and the sum of the number of antennas plus one nearly remains fixed, which is insensitive to different system configurations. With the number of active users set as the optimal number, ASE increases linearly with the number of antennas of both tier.
- If the number of antennas of MBSs is sufficiently larger than that of SBSs, range expansion will improve ASE. Besides, the region of the number of antennas where range expansion improves ASE is insensitive to $\frac{\lambda_s}{\lambda_m}$. However, larger $\frac{P_s}{P_m}$ will expand the improvement region.

II. SYSTEM MODEL

We consider a downlink two-tier network where the macro tier is overlaid with co-channel deployed SBSs. The positions of MBSs and SBSs are modeled as PPPs Φ_m, Φ_s with density λ_m, λ_s . The MBSs and SBSs have transmit power P_m, P_s and are equipped with M_m, M_s antennas. The single-antenna users are located according to some stationary point process, which is independent of Φ_m, Φ_s . We adopt standard path

¹ $\frac{\lambda_s}{\lambda_m}, \frac{P_s}{P_m}$ are the ratios of BS density, transmit power between MBSs and SBSs, which will be defined in the main body of this paper.

loss propagation model with path loss exponent $\alpha > 2$. User association is based on the long-term average biased received power. The range expansion bias for SBSs is B .

Each MBS and SBS serves K_m, K_s active users at each slot. We consider zero-forcing (ZF) precoding and assume perfect channel state information at each BS. Thus, we have $K_m \leq M_m, K_s \leq M_s$. We follow the infinite user density assumption in [8][10]. Therefore, there are at least K_m, K_s users covered by each MBS and SBS. The transmit power is allocated equally for the active users in each cell. The small scale fading on each link is i.i.d. Rayleigh fading. The thermal noise is ignored in this paper. Without loss of generality, we will focus on the analysis of a typical user located at the origin [12]. The signal-to-noise-ratio (SIR) of the typical user located at the origin is

$$SIR_l = \frac{\frac{P_l g_{l0}}{K_l \|x_0\|^\alpha}}{\sum_{x_i \in \Phi_m \setminus \{x_0\}} \frac{P_m h_{mi}}{K_m \|x_i\|^\alpha} + \sum_{x_i \in \Phi_s \setminus \{x_0\}} \frac{P_s h_{si}}{K_s \|x_i\|^\alpha}}, \quad (1)$$

where x_0 indicates the BS the typical user associated with, and $l = m, s$ depends on which type BS x_0 is. According to [8][10], we know the equivalent channel gains $g_{l0} \sim \text{Gamma}(M_l + 1 - K_l, 1)$, $h_{mi} \sim \text{Gamma}(K_m, 1)$ and $h_{si} \sim \text{Gamma}(K_s, 1)$.²

III. ANALYSIS OF THE TYPICAL USER

In this section, we will study the average data rate of the typical user, especially, the impact of different configurations between two tiers will be discussed.

A. Theoretical Analysis

Taking average over spatial distribution and channel power distribution, we can obtain the average data rate of the typical user, which is provided in the following theorem.

Theorem 1: The average data rate R_m, R_s of the typical user in macro tier and small cell tier are given by

$$\begin{aligned} R_m &= \int_0^\infty \frac{\left(1 + \frac{\lambda_s}{\lambda_m} \left(\frac{P_s B}{P_m}\right)^{2/\alpha}\right) \left(1 - \left(\frac{1}{1+z}\right)^{M_m+1-K_m}\right)}{z \left(F(z, K_m) + \frac{\lambda_s}{\lambda_m} \left(\frac{P_s B}{P_m}\right)^{2/\alpha} F\left(\frac{z K_m}{K_s B}, K_s\right)\right)} dz, \\ R_s &= \int_0^\infty \frac{\left(\frac{\lambda_m}{\lambda_s} \left(\frac{P_m}{P_s B}\right)^{2/\alpha} + 1\right) \left(1 - \left(\frac{1}{1+z}\right)^{M_s+1-K_s}\right)}{z \left(\frac{\lambda_m}{\lambda_s} \left(\frac{P_m}{P_s B}\right)^{2/\alpha} F\left(\frac{z K_s B}{K_m}, K_m\right) + F(z, K_s)\right)} dz, \end{aligned} \quad (2)$$

where $F(x, y) = 1 + x^{2/\alpha} \int_{x^{-2/\alpha}}^\infty \left(1 - (1 + u^{-\alpha/2})^{-y}\right) du$.

Proof: The proof is given in the appendix. ■

Theorem 1 provide tractable expressions for the average data rate of users in multi-antenna two-tier networks. However, R_m, R_s have complicated relationships with other system parameters. To further study how the differences between two tiers impact on the network performance, we provide more tractable approximations for R_m, R_s , which are demonstrated to be quite tight in our numerical results.

Theorem 2: The approximations for R_m, R_s are

$$\begin{aligned} \tilde{R}_m &= \int_0^\infty \frac{1}{z} \frac{\left(1 + \frac{\lambda_s}{\lambda_m} \left(\frac{P_s B}{P_m}\right)^{2/\alpha}\right) \left(1 - e^{-z \frac{M_m+1-K_m}{K_m}}\right)}{H(z) + \frac{\lambda_s}{\lambda_m} \left(\frac{P_s B}{P_m}\right)^{2/\alpha} H\left(\frac{z}{B}\right)} dz, \\ \tilde{R}_s &= \int_0^\infty \frac{1}{z} \frac{\left(\frac{\lambda_m}{\lambda_s} \left(\frac{P_m}{P_s B}\right)^{2/\alpha} + 1\right) \left(1 - e^{-z \frac{M_s+1-K_s}{K_s}}\right)}{\frac{\lambda_m}{\lambda_s} \left(\frac{P_m}{P_s B}\right)^{2/\alpha} H(zB) + H(z)} dz, \end{aligned} \quad (3)$$

²Actually, the proposition h_{mi}, h_{si} are Gamma distributed is an accurate approximation, which is widely adopted in previous works [6][8][9][10].

where $H(x) = 1 + x^{2/\alpha} \int_{x^{-2/\alpha}}^\infty (1 - \exp(-u^{-\alpha/2})) du$.

Proof: The proof is given in the appendix. ■

From Theorem 1, R_m, R_s are unrelated to the number of antennas of the other tier. Interestingly, besides the number of antennas, \tilde{R}_m, \tilde{R}_s do not depend on the number of active users of the other tier either. In fact, numerical results show that the original expressions R_m, R_s are also insensitive to the number of active users of the other tier, i.e., R_m, R_s behave similarly to \tilde{R}_m, \tilde{R}_s . Moreover, based on Theorem 1, we find that the ratios $\frac{\lambda_s}{\lambda_m}, \frac{P_s}{P_m}$ and B mainly affect \tilde{R}_m, \tilde{R}_s .

Lemma 1: When $B > 1$, we have 1) \tilde{R}_m increases with $\frac{\lambda_s}{\lambda_m}, \frac{P_s}{P_m}$, and B ; 2) \tilde{R}_s increases with $\frac{\lambda_s}{\lambda_m}$ and $\frac{P_s}{P_m}$, but decreases with B . However, when $B = 1$, \tilde{R}_m, \tilde{R}_s are unrelated to $\lambda_s, \lambda_m, P_s, P_m$ and can be simplified as

$$\tilde{R}_m = \int_0^\infty \frac{1 - e^{-z \frac{M_m+1-K_m}{K_m}}}{z H(z)} dz, \quad \tilde{R}_s = \int_0^\infty \frac{1 - e^{-z \frac{M_s+1-K_s}{K_s}}}{z H(z)} dz.$$

Proof: The proof is given in the appendix. ■

It is a well-known fact that the average data rate increases with B for macro users, but decreases with B for small cell users. However, instead of numerical results, this property is demonstrated theoretically through the tight approximations in this paper. Furthermore, it is interesting to point out that both \tilde{R}_m, \tilde{R}_s increase with $\frac{\lambda_s}{\lambda_m}$ and $\frac{P_s}{P_m}$ when $B > 1$, which has never been reported in previous works. That is to say, the more small cells or the higher transmit power of small cells, the average data rate of both tiers will be larger. Another interesting result is that the approximations of users' data rate do not depend on BS density nor BS transmit power when $B = 1$, which is similar to the single-antenna scenario [4]. The properties in Lemma 1 will be validated for the original expressions R_m, R_s through numerical results.

Fig. 1 depicts R_m, R_s with different system parameters. We can find that the approximations in Theorem 2 is quite accurate. Moreover, all the mentioned properties of \tilde{R}_m, \tilde{R}_s are validated for R_m, R_s . Firstly, we find R_m, R_s are insensitive to the number of active users of the other tier. The reason is that, instead of K_m, K_s , it is the total powers P_m, P_s which dominate the cross-tier interference. Secondly, when $B > 1$, we observe that both R_m and R_s increase with $\frac{\lambda_s}{\lambda_m}, \frac{P_s}{P_m}$. By increasing λ_s , we know that the inter-cell interference from the small cell tier will be stronger. However, the users will be closer to the associated BSs, which makes the desired signal power stronger. From Fig. 1, we know that the increase of desired signal power is larger than the increase of the interference power, which leads to the fact that R_m, R_s increases with $\frac{\lambda_s}{\lambda_m}$. Similarly, for increasing P_s , we also know that the increase of desired power is larger than the interference power. Different from the case $B > 1$, when $B = 1$, R_m, R_s are insensitive to $\frac{\lambda_s}{\lambda_m}$ and $\frac{P_s}{P_m}$. That is to say, when $B = 1$, the increase of desired signal power due to large λ_s, P_s is counter-balanced by the increase of inter-cell interference. Comparing the results for $B = 4$ and $B = 1$, we find range expansion will improve R_m but degrade R_s . This property is similar to the single-antenna HetNets [4]. However, we consider a more general case where multi-antenna BSs are considered. Above all, all theoretical results based on the approximations \tilde{R}_m, \tilde{R}_s are validated for R_m, R_s . The impact of differences between two tiers on users' data rate has been revealed.

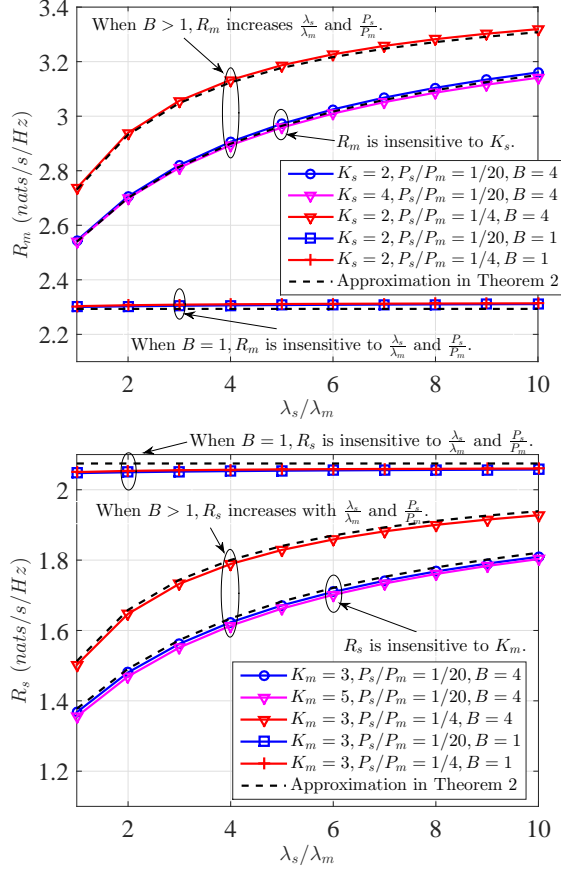


Fig. 1. R_m, R_s with different system parameters. $\alpha = 4$. In the figure R_m , we set $M_m = 10, K_m = 3$. In the figure R_s , we set $M_s = 5, K_s = 2$.

IV. AREA SPECTRAL EFFICIENCY OPTIMIZATION

In this section, we will study the optimal K_m^*, K_s^* to maximize ASE. The key properties of K_m^*, K_s^* under different system parameters will be revealed. How range expansion affects ASE will be discussed.

A. The Optimal Number of Active Users

Based on Theorem 1, the expression of ASE can be expressed as $T = \lambda_m K_m R_m + \lambda_s K_s R_s$. We find that K_m, K_s are crucial system design parameters, which affect ASE of both tiers. Thus, we attempt to obtain the optimal K_m^*, K_s^* to maximize ASE. It is difficult to maximize T directly because of the complex expressions of R_m, R_s . Therefore, we obtain $\tilde{K}_m^*, \tilde{K}_s^*$ that maximize the approximations $\tilde{T} = \lambda_m K_m \tilde{R}_m + \lambda_s K_s \tilde{R}_s$ instead. Fortunately, due to the tightness of the approximations, the numerical results demonstrate that the results based on the \tilde{T} are consistent with T .

In detail, we formulate the following problem,

$$\begin{aligned} \max_{K_m, K_s} \quad & \lambda_m K_m \tilde{R}_m + \lambda_s K_s \tilde{R}_s \\ \text{s.t.} \quad & K_m \in \{0, 1, \dots, M_m\}, K_s \in \{0, 1, \dots, M_s\}. \end{aligned} \quad (4)$$

Substituting $u_m = \frac{K_m}{M_m+1}, u_s = \frac{K_s}{M_s+1}$ into the above problem and relaxing u_m, u_s to $[0, 1]$, we arrive at the following

problem,

$$\begin{aligned} \max_{u_m, u_s} \quad & \lambda_m (M_m + 1) G_m(u_m) + \lambda_s (M_s + 1) G_s(u_s) \\ \text{s.t.} \quad & u_m, u_s \in [0, 1]. \end{aligned} \quad (5)$$

where $G_m(u) = \int_0^\infty \frac{u(1 + \frac{\lambda_s}{\lambda_m} (\frac{P_s B}{P_m})^{2/\alpha}) (1 - e^{-z/u+uz})}{z(H(z) + \frac{\lambda_s}{\lambda_m} (\frac{P_s B}{P_m})^{2/\alpha} H(\frac{z}{B}))} dz$, $G_s(u) = \int_0^\infty \frac{u(\frac{\lambda_m}{\lambda_s} (\frac{P_m}{P_s B})^{2/\alpha} + 1) (1 - e^{-z/u+uz})}{z(\frac{\lambda_m}{\lambda_s} (\frac{P_m}{P_s B})^{2/\alpha} H(zB) + H(z))} dz$. For the optimization problem (5), we have the following observations.

- Firstly, u_m, u_s can be optimized separately to maximize $G_m(u), G_s(u)$.
- Secondly, the optimal u_m^*, u_s^* do not depend M_m, M_s , i.e., for arbitrary M_m, M_s , the optimal numbers of active users are $(M_m + 1) u_m^*, (M_s + 1) u_s^*$.
- Furthermore, with the optimal u_m^*, u_s^* , the approximations of ASE $\tilde{T}^* = \lambda_m (M_m + 1) G_m(u_m^*) + \lambda_s (M_s + 1) G_s(u_s^*)$, which will increase linearly with M_m, M_s .

Through the second order derivatives, it is not difficult to show that both $G_m(u)$ and $G_s(u)$ are concave function of u . Therefore, the optimal u_m^*, u_s^* can be obtained by setting first order derivative as zero.

Theorem 3: u_m^* is the solution of $\int_0^\infty \frac{1 - e^{-z/u+uz} - \frac{z}{u} e^{-z/u+uz}}{z(H(z) + \frac{\lambda_s}{\lambda_m} (\frac{P_s B}{P_m})^{2/\alpha} H(\frac{z}{B}))} dz = 0$. u_s^* is the solution of $\int_0^\infty \frac{1 - e^{-z/u+uz} - \frac{z}{u} e^{-z/u+uz}}{z(\frac{\lambda_m}{\lambda_s} (\frac{P_m}{P_s B})^{2/\alpha} H(zB) + H(z))} dz$. Both of the two equations have a unique solution located in $[0, 1]$, which can be obtained through the bisection method.

Proof: We take u_m as an example. Take the first order derivative $\frac{\partial}{\partial u} G_m(u)$, we arrive at the mentioned equation. $\frac{\partial}{\partial u} G_m(u)$ is a decreasing function of u . Besides, for the boundaries 0, 1, it is not difficult to show that $\lim_{u \rightarrow 0} \frac{\partial}{\partial u} G_m(u) = \int_0^\infty \frac{1}{z(H(z) + \frac{\lambda_s}{\lambda_m} (\frac{P_s B}{P_m})^{2/\alpha} H(\frac{z}{B}))} dz > 0$ and $\frac{\partial}{\partial u} G_m(1) = - \int_0^\infty \frac{1}{(H(z) + \frac{\lambda_s}{\lambda_m} (\frac{P_s B}{P_m})^{2/\alpha} H(\frac{z}{B}))} dz < 0$. Therefore, there is a unique solution located in $[0, 1]$, which can be solved through bisection method. ■

From Theorem 3, after rounding $(M_m + 1) u_m^*$ and $(M_s + 1) u_s^*$, we can obtain the optimal $\tilde{K}_m^*, \tilde{K}_s^*$ that maximizes \tilde{T} . Interestingly, although it is obvious that $\tilde{K}_m^*, \tilde{K}_s^*$ depends on $\frac{\lambda_s}{\lambda_m}, \frac{P_s}{P_m}$ and B , we find that $\tilde{K}_m^*, \tilde{K}_s^*$ are insensitive to these parameters in numerical results. The optimality of $\tilde{K}_m^*, \tilde{K}_s^*$ for the original expression T will be also validated through numerical results.

B. Numerical Illustrations

By exhaustive search, we obtain the optimal K_m^*, K_s^* that maximizes T . Fig. 2 illustrates K_m^*, K_s^* under different system parameters. It is obvious that K_m^* is either $\lfloor u_m^* (M_m + 1) \rfloor$ or $\lceil u_m^* (M_m + 1) \rceil$, K_s^* is either $\lfloor u_s^* (M_s + 1) \rfloor$ or $\lceil u_s^* (M_s + 1) \rceil$. That is to say, the solution based \tilde{T} can be applied to T directly. Interestingly, we find u_m^*, u_s^* is always located in $[0.59, 0.64]$ even under different system parameters. Therefore, the optimal K_m^*, K_s^* are

³In fact, the number of active users should be rounded.

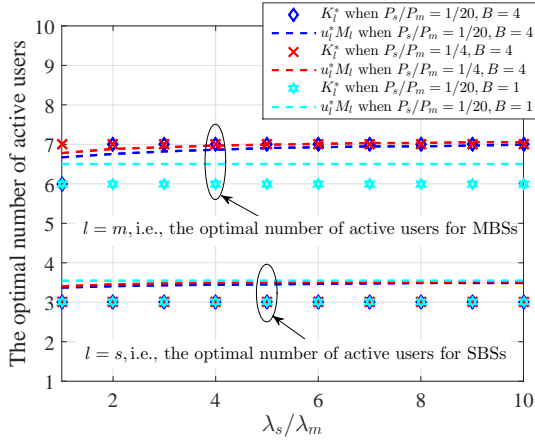


Fig. 2. The optimal number of active users. $M_m = 10$, $M_s = 5$, $\alpha = 4$.

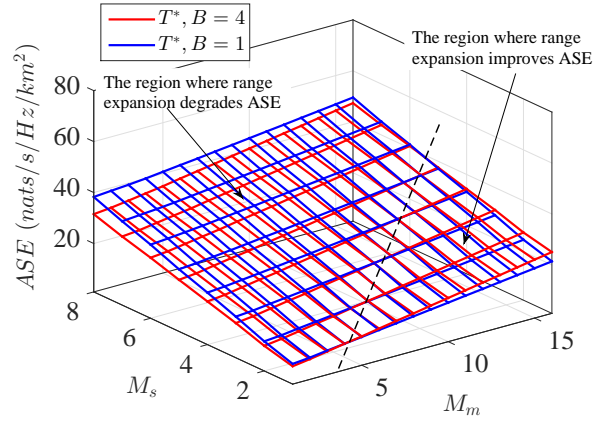


Fig. 4. T^* with respect to M_m , M_s , B . $\frac{\lambda_s}{\lambda_m} = 5$, $\frac{P_s}{P_m} = \frac{1}{20}$, $\alpha = 4$.

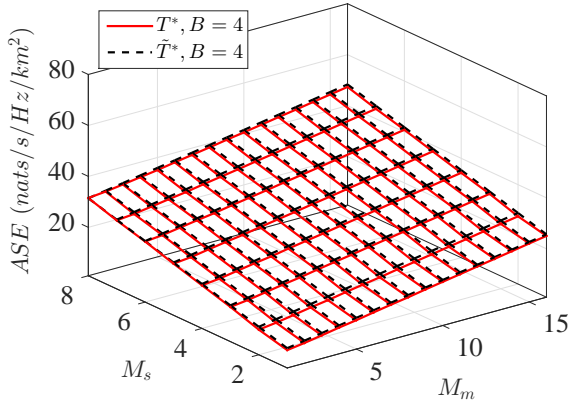


Fig. 3. T^* , \tilde{T}^* with respect to M_m , M_s . $\frac{\lambda_s}{\lambda_m} = 5$, $\frac{P_s}{P_m} = \frac{1}{20}$, $\alpha = 4$.

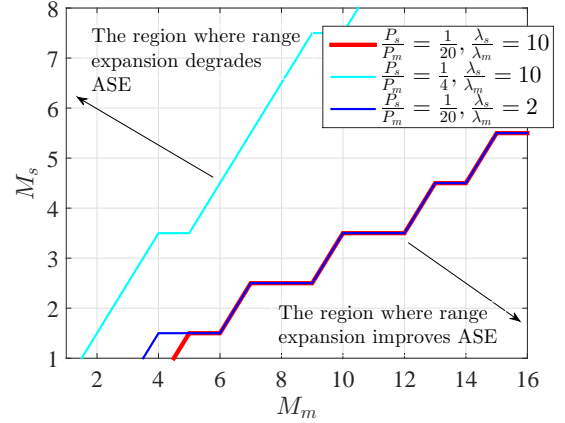


Fig. 5. The range expansion improvement/degradation region. $\alpha = 4$.

insensitive to different configurations between the two tiers. Specifically, $K_m^* = 6$ or 7 and $K_s^* = 3$ for different $\frac{\lambda_s}{\lambda_m}$, $\frac{P_s}{P_m}$, B .

When the number of active users set as optimal, Fig. 3 depicts T , \tilde{T} with respect to M_m , M_s . We find the mismatch between \tilde{T}^* and T^* is quite small, which demonstrates the tightness of Theorem 2. As we mentioned in subsection A, with optimal u_m^* and u_s^* , \tilde{T} will increase linearly with M_m , M_s . Consistent with T^* , we can see that T^* also increases linearly with M_m , M_s . The reasons for this phenomenon are as follows. From Theorem 3, we know that K_m^* , K_s^* are approximately fixed portion of $M_m + 1$, $M_s + 1$, respectively. In such situation, from Theorem 2, we know that R_m , R_s nearly remain fixed for different M_m , M_s . However, the number of active users K_m^* , K_s^* will increase linearly with M_m , M_s . In summary, T^* will increase linearly with M_m , M_s .

With the optimal K_m^* , K_s^* , Fig. 4 depicts T^* with M_m , M_s considering different range expansion bias B . In single-antenna HetNets, it is found that range expansion will degrade the overall ASE [4]. However, it is not true for multi-antenna HetNets. From Fig. 4, if M_m is sufficiently larger than M_s , range expansion will improve the ASE. The reasons are as follows. As we mentioned in Theorem 2, range expansion

will improve R_m but degrade R_s . If M_m is sufficiently larger than M_s , the value of R_m will be sufficiently larger than R_s . Hence, R_m will benefit more from range expansion. Besides, as $K_m^* \approx u_m^*(M_m + 1)$, the larger M_m is, the more macro users will benefit from the range expansion. Thus, the improvement of $\lambda_m K_m R_m$ due to range expansion will make up for the degradation of $\lambda_s K_s R_s$. Fig. 5 illustrate the regions where range expansion improves or degrades ASE under different system parameters. It is interesting to point out that, the improvement/degradation region is insensitive to $\frac{\lambda_s}{\lambda_m}$. Instead, the difference in transmit power $\frac{P_s}{P_m}$ significantly affects the improvement/degradation region. Specifically, the large $\frac{P_s}{P_m}$ is, the improvement region will be larger. Based on Theorem 2, we know that increasing $\frac{P_s}{P_m}$ improves both R_m , R_s . However, from Fig. 5, we know that the improvement of $\lambda_m K_m R_m$ is larger than that of $\lambda_s K_s R_s$, which leads to the fact that the improvement region will be expanded with the increase of $\frac{P_s}{P_m}$.

V. CONCLUSIONS

In this paper, we have studied the users' average data rate and the optimal settings in multi-antenna two-tier networks. With the help of the tractable approximations, the key proper-

ties of system performance have been revealed. We find that the users' data rate of each tier is insensitive to the number of active users of the other tier. If $B > 1$, we find users' data rate increases with $\frac{\lambda_s}{\lambda_m}, \frac{P_s}{P_m}$. However, if $B = 1$, the users' data rate is insensitive to $\frac{\lambda_s}{\lambda_m}, \frac{P_s}{P_m}$. For the purpose of ASE maximization, we find the optimal number of active users of each tier is fixed portion of the sum of the number of antennas plus one. The optimal settings are insensitive to different system parameters. With optimal settings, ASE will increase linearly with the number of antennas. Moreover, we find that, if the number of antennas of MBSs is sufficiently larger than SBSs, range expansion will improve ASE. The improvement region will expand with larger $\frac{P_s}{P_m}$.

This work has revealed the key properties of multi-antenna two-tier networks. Further extension of this work is to consider more sophisticated multi-antenna techniques, such as coordinated beamforming and transmit-receive diversity.

APPENDIX

Proof of Theorem 1: We follow the similar approach with [13]. However, we obtain much more simple expressions for multi-antenna HetNets. Take R_m as an example. $E[\log(1 + SIR_m)] = \int_0^\infty f_m(r) E[\log(1 + SIR_m)|r] dr$, where $f_m(r) = 2\pi r \left(\lambda_m + \lambda_s \left(\frac{P_s B}{P_m} \right)^{2/\alpha} \right) e^{-\lambda_m \pi r^2 - \lambda_s \pi \left(\frac{P_s B}{P_m} \right)^{2/\alpha} r^2}$ is the distance distribution between the macro user and the serving MBS x_0 [4]. Following the lemma in [14], $E[\log(1 + SIR_m)|r] = \int_0^\infty \frac{1 - \mathcal{L}_{g_{m0}}(z)}{z} \mathcal{L}_{\bar{I}_m}(z) \mathcal{L}_{\bar{I}_s}(z) dz$, where $\bar{I}_m = \sum_{x_i \in \Phi_m \setminus \{x_0\}} \frac{h_{mi} r^\alpha}{\|x_i\|^\alpha}$ and $\bar{I}_s = \sum_{x_i \in \Phi_s} \frac{P_s K_m h_{mi} r^\alpha}{P_m K_s \|x_i\|^\alpha}$. As g_{m0} is Gamma distributed, we have $\mathcal{L}_{g_{m0}}(z) = (1/(1+z))^{M_m+1-K_m}$. From the properties of PPP, we have $\mathcal{L}_{\bar{I}_m}(z) = e^{-\lambda_m \pi r^2 (F(z, K_m) - 1)}$, $\mathcal{L}_{\bar{I}_s}(z) = e^{-\lambda_s \pi r^2 \left(\frac{P_s B}{P_m} \right)^{2/\alpha} (F(\frac{z K_m}{K_s B}, K_s) - 1)}$. Above all, substituting $E[\log(1 + SIR_m)|r]$ into the primary integral, we can derive R_m after some algebraic manipulations. ■

Proof of Theorem 2: The main procedures are similar to Theorem 1, except that we derive an approximation for $E[\log(1 + SIR_m)|r]$ by averaging the equivalent channel gains g_{m0} , h_{mi} and h_{si} . Specifically, we have

$$\begin{aligned} & E[\log(1 + SIR_m)|r] \\ & \approx E_{\Phi_m, \Phi_s} \left[\log \left(1 + \frac{\frac{P_m E[g_{m0}]}{K_m r^\alpha}}{\sum_{x_i \in \Phi_m \setminus \{x_0\}} \frac{P_m E[h_{mi}]}{K_m \|x_i\|^\alpha} + \sum_{x_i \in \Phi_s} \frac{P_s E[h_{si}]}{K_s \|x_i\|^\alpha}} \right) \right] \\ & = E_{\Phi_m, \Phi_s} \left[\log \left(1 + \frac{\frac{M_m + 1 - K_m}{K_m}}{\sum_{x_i \in \Phi_m \setminus \{x_0\}} \frac{r^\alpha}{\|x_i\|^\alpha} + \sum_{x_i \in \Phi_s} \frac{P_s r^\alpha}{P_m \|x_i\|^\alpha}} \right) \right] \\ & = \int_0^\infty \frac{1 - e^{-z \frac{M_m + 1 - K_m}{K_m}}}{z} e^{-\lambda_m \pi r^2 (H(z) - 1) - \lambda_s \left(\frac{P_s B}{P_m} \right)^{2/\alpha} \pi r^2 (H(z/B) - 1)} dz. \end{aligned} \quad (6)$$

Proof of Lemma 1: First consider the case $B > 1$. We first show \tilde{R}_m increases with $\frac{\lambda_s}{\lambda_m}$ and $\frac{P_s}{P_m}$. Let $t = \frac{\lambda_s}{\lambda_m} \left(\frac{P_s}{P_m} \right)^{2/\alpha}$. Based on Leibniz integral rule, we only need to prove the integral item $\frac{1 + \frac{\lambda_s}{\lambda_m} \left(\frac{P_s B}{P_m} \right)^{2/\alpha}}{H(z) + \frac{\lambda_s}{\lambda_m} \left(\frac{P_s B}{P_m} \right)^{2/\alpha} H\left(\frac{z}{B}\right)}$

increases with t . Take the first order derivative, we have $\frac{\partial}{\partial t} \left(\frac{1 + B^{2/\alpha} t}{H(z) + t B^{2/\alpha} H\left(\frac{z}{B}\right)} \right) = \frac{B^{2/\alpha} (H(z) - H\left(\frac{z}{B}\right))}{\left(H(z) + t B^{2/\alpha} H\left(\frac{z}{B}\right) \right)^2}$. We find $H(x)$ increases with x , i.e., $H(x) > H\left(\frac{x}{B}\right)$. Thus, $\frac{\partial}{\partial t} \left(\frac{1 + B^{2/\alpha} t}{H(z) + t B^{2/\alpha} H\left(\frac{z}{B}\right)} \right) > 0$. Therefore, \tilde{R}_m increases with $\frac{\lambda_s}{\lambda_m}$ and $\frac{P_s}{P_m}$. Similarly, we can prove \tilde{R}_s increases with $\frac{\lambda_s}{\lambda_m}$ and $\frac{P_s}{P_m}$. Then, we will prove R_m increase with B . Indeed, we have $\frac{\partial}{\partial B} \left(\frac{1 + B^{2/\alpha} t}{H(z) + t B^{2/\alpha} H\left(\frac{z}{B}\right)} \right) = \frac{2t B^{2/\alpha - 1} H(z) - e^{-\frac{z}{B}} + t B^{2/\alpha} \left(H\left(\frac{z}{B}\right) - e^{-\frac{z}{B}} \right)}{\alpha \left(H(z) + t B^{2/\alpha} H\left(\frac{z}{B}\right) \right)^2}$. It is obvious that $H(x) > 1$ and $e^{-\frac{z}{B}} < 1$. Thus, $\frac{\partial}{\partial B} \left(\frac{1 + B^{2/\alpha} t}{H(z) + t B^{2/\alpha} H\left(\frac{z}{B}\right)} \right) > 0$, i.e., \tilde{R}_m increases with B . Following similar procedures, we can prove \tilde{R}_s decreases with B . For the case $B = 1$, the results can be obtained easily by substituting $B = 1$. ■

REFERENCES

- [1] N. Bhushan, J. Li, D. Malladi, R. Gilmore, D. Brenner, A. Damjanovic, R. T. Sukhvasi, C. Patel, S. G. Gehofer, "Network densification: the dominant theme for wireless evolution into 5G," *IEEE Commun. Mag.*, vol. 52, no. 2, pp. 82-89, Feb. 2014.
- [2] S. Mukherjee, "Distribution of downlink SINR in heterogeneous cellular networks," *IEEE J. Sel. Areas Commun.*, vol. 30, no. 3, pp. 575-585, Apr. 2012.
- [3] H. S. Dhillon, R. K. Ganti, F. Baccelli, and J. G. Andrews, "Modeling and analysis of K-Tier downlink heterogeneous cellular networks," *IEEE J. Sel. Areas Commun.*, vol. 30, no. 2, pp. 550-560, Apr. 2012.
- [4] H. Jo, Y. J. Sang, P. Xia, and J. G. Andrews, "Heterogeneous cellular networks with flexible cell association: a comprehensive downlink SINR analysis," *IEEE Trans. Wireless Commun.*, vol. 11, no. 10, pp. 3484-3495, Oct. 2012.
- [5] C. Li, J. Zhang, and K. B. Letaief, "Throughput and energy efficiency analysis of small cell networks with multi-antenna base stations," *IEEE Trans. Wireless Commun.*, vol. 13, no. 5, pp. 2505-2517, May 2014.
- [6] Z. Chen, L. Qiu, and X. Liang, "Area spectral efficiency analysis and energy consumption minimization in multi-antenna Poisson distributed networks," available at <http://arxiv.org/abs/1601.01376>
- [7] M. D. Renzo, and W. Lu, "Stochastic geometry modeling and performance evaluation of MIMO cellular networks using equivalent-in-distribution(EID)-based approach," *IEEE Trans. Commun.*, vol. 63, no. 3, pp. 977-996, Mar. 2015.
- [8] H. S. Dhillon, M. Kountouris, and J. G. Andrews, "Downlink MIMO HetNets: modeling, ording results and performance analysis," *IEEE Trans. Wireless Commun.*, vol. 13, no. 10, pp. 5208-5222, Oct. 2013.
- [9] A. K. Gupta, H. S. Dhillon, S. Vishwanath, J. G. Andrews, "Downlink multi-antenna heterogeneous cellular network with load balancing," *IEEE Trans. Commun.*, vol. 62, no. 11, pp. 4052-4067, Nov. 2014.
- [10] C. Li, J. Zhang, J. G. Andrews, and K. B. Lataief, "Success probability and area spectral efficiency in multiuser MIMO HetNets," available at <http://arxiv.org/pdf/1506.05197v1.pdf>.
- [11] R. Tanbourgi, H. S. Dhillon, and F. K. Jondral, "Analysis of joint transmit-receive diversity in downlink MIMO heterogeneous cellular networks," *IEEE Trans. Wireless Commun.*, vol. 14, no. 12, pp. 6695-6709, Dec. 2015.
- [12] F. Baccelli, and B. Blaszczyszyn, *Stochastic Geometry and Wireless Networks - Volume I: Theory*, Foundations and Trends in Networking, 2009.
- [13] M. D. Renzo, A. Guidotti, G. E. Corazza, "Average rate of downlink heterogeneous cellular networks over generalized fading channels: a stochastic geometry approach," *IEEE Trans. Commun.*, vol. 61, no. 7, pp. 3050-3071, Jul. 2013.
- [14] K. A. Hamdi, "A useful lemma for capacity analysis of fading interference channels," *IEEE Trans. Commun.*, vol. 58, no. 2, pp. 411-416, Feb. 2010.